Lawrence Berkeley National Laboratory
Recent Work

Title

Submillimeter and Microwave Residual Losses in Epitaxial Films of Y-Ba-Cu-O and Tl-Ca-Ba-Cu-O

Permalink

https://escholarship.org/uc/item/1v1238wp

Authors

Miller, D.
Richards, P.L.
Garrison, S.M.
et al.

Publication Date

1992-03-01

Center for Advanced Materials

CAM

Presented at the Second Symposium on High Temperature
Superconductors in High Frequency Fields, Santa Fe, NM,
April 1-3, 1992, and to be published in the Proceedings

Submillimeter and Microwave Residual Losses
in Epitaxial Films Y-Ba-Cu-O and Tl-Ca-Ba-Cu-O

D. Miller, P.L. Richards, S.M. Garrison, N. Newman, C.B. Eom,
T.H. Geballe, S. Etemad, A. Inam, T. Venkatesan, J.S. Martens,
W.Y. Lee, and L.C. Bourne

March 1992
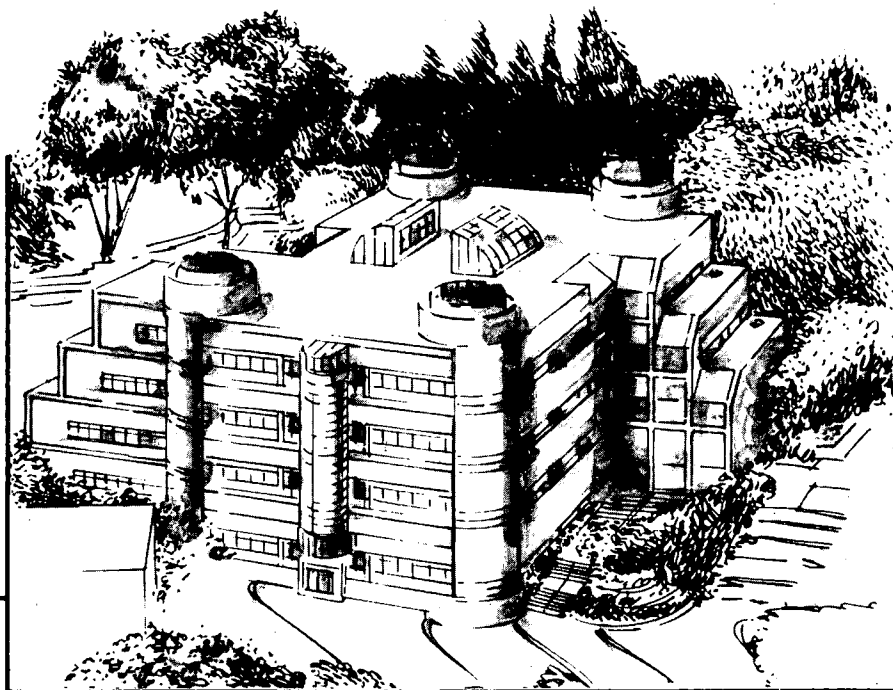
Materials and Chemical Sciences Division

Lawrence Berkeley Laboratory • University of California
ONE CYCLOTRON ROAD, BERKELEY, CA 94720 • (415) 486-4755

DISCLAIMER

Submillimeter and Microwave Residual Losses in Epitaxial Films of Y-Ba-Cu-O and Tl-Ca-Ba-Cu-O

D. MILLER, P.L. RICHARDS

Department of Physics, University of California, and Materials Sciences Division, Lawrence Berkeley Laboratory,Berkeley CA 94720

S.M. GARRISON, N. NEWMAN

Conductus, Inc., Sunnyvale, CA 94086

C.B. EOM, T.H. GEBALLE

Department of Applied Physics, Stanford University, Stanford CA 94305

S. ETEMAD, A. INAM, T. VENKATESAN

Bell Communications Research, Red Bank, New Jersey 07701

J.S. MARTENS

Sandia National Laboratory, Albuquerque NM 87185

W.Y. LEE

IBM Almaden, San Jose CA 95120

L.C. BOURNE

Superconductor Technologies, Santa Barbara CA 93111

Abstract

We have used a novel bolometric technique and a resonant technique to obtain accurate submillimeter and microwave residual loss data for epitaxial thin films of $YBa_2Cu_3O_7$, $Tl_2Ca_2Ba_2Cu_3O_{10}$ and $Tl_2CaBa_2Cu_2O_8$. For all films we obtain good agreement between the submillimeter and microwave data, with the residual losses in both the Y-Ba-Cu-O and Tl-Ca-Ba-Cu-O films scaling aproximately as frequency squared below ~ 1 THz. We are able to fit the losses in the Y-Ba-Cu-O films to a weakly coupled grain model for the a-b plane conductivity, in good agreement with results from a Kramers-Kronig analysis of the loss data. We observe strong phonon structure in the Tl-Ca-Ba-Cu-O films for frequencies between 2 and 21 THz, and are unable to fit these losses to the simple weakly coupled grain model. This is in strong contrast to the case for other high T_c superconductors such as $YBa_2Cu_3O_7$, where phonon structure observed in ceramic samples is absent in epitaxial oriented films and crystals because of the electronic screening due to the high conductivity of the a-b planes.

Keywords: superconductivity, ac losses, Y-Ba-Cu-O, Tl-Ca-Ba-Cu-O

1. Introduction

A knowledge of the residual losses at microwave, millimeter and submillimeter frequencies plays an important role in our understanding of the superconducting state properties of the high-T_c superconductors. In addition to aiding in our understanding of the superconducting electrodynamics of these materials, it is essential to have a good understanding of the low frequency losses for microwave device applications. However, there remains a lack of a consistent picture of the loss spectrum between microwave and submillimeter frequencies.

While microwave experiments typically involve measurements of the surface resistance, R_S, or equivalently the absorbed power, A, conventional submillimeter experiments typically involve measurements of the reflectivity, R. For optically thick samples, absorptivity and reflectivity measurements are simply related by A = 1 - R and in principle provide equivalent spectral information. However, at low temperatures and for frequencies below ~10 THz the reflectivity of the high T_c materials approaches unity. In this case, systematic errors, such as drift, standing waves, and sample placement errors, which tend to multiply the measured spectral information, can then cause the measured reflectivity to become less reliable than the measured absorptivity. For these reasons there is a significant advantage of a direct absorptivity measurement over reflectivity measurements when the sample reflectivities being studied are close to unity. Also, uncertainties associated with the precise determination of unity reflectivity are minimized by measuring the absorptivity directly. In addition, direct absorptivity measurements are less sensitive to substrate properties than transmissivity measurements.

In order to improve the accuracy of the submillimeter data we have developed a novel technique for directly measuring this residual loss.[1,2] In this technique the high-T_c film is used as the absorber in a composite bolometric detector. Our technique allows us to obtain accurate direct absorptivity data on epitaxial a-b plane films in the frequency range between microwave loss and infrared reflectivity measurements. Similar techniques have been used by others to measure absorptivity in single crystals of $YBa_2Cu_3O_7$.[3,4] In this paper we present data for five $YBa_2Cu_3O_7$ films, one $Tl_2CaBa_2Cu_2O_8$ film and two mixed phase $Tl_2Ca_2Ba_2Cu_3O_{10}$ and $Tl_2CaBa_2Cu_2O_8$ films.[1,2] The residual losses in the $YBa_2Cu_3O_7$ films used for this study were also measured near 10 GHz using microwave cavity techniques, and are among the lowest reported in the literature. The residual losses in the Tl-Ca-Ba-Cu-O films used in this study were measured

near 10 GHz using microwave cavity techniques[5,6] and near 30 and 90 GHz using a confocal resonator technique.[7] Using the well documented frequency squared dependence of the microwave loss up to 100 GHz,[8] we can infer the loss in our films over four decades in frequency.

One of the most studied cuprate superconductors is the $T_c \sim 90$ K material $YBa_2Cu_3O_7$. Microwave measurements show a temperature dependent component to the loss similar to that for a BCS superconductor plus a substantial residual loss that remains at low temperatures. This residual loss is minimized in high quality epitaxial a-b plane films. Both contributions to the loss vary as frequency squared from ~10 to ~100 GHz. Reflectivity measurements on twinned epitaxial films at submillimeter wavelengths show that the losses increase slowly with frequency up to an absorption edge at 13.5 THz (450 cm^{-1}). Although not as heavily investigated, the thallium based materials show similar microwave frequency and temperature dependences.[8] Reflectivity measurements on epitaxial $Tl_2CaBa_2Cu_2O_8$ films are similar to the best $YBa_2Cu_3O_7$ films.[9]

The absorptivities we have measured for the $YBa_2Cu_3O_7$ films in this study vary as frequency squared up to ~ 300 GHz (10 cm^{-1}) and then approaches a constant by 450 cm^{-1} where there is a sharp onset of additional absorption. We do not observe any absorption onset at 140 cm^{-1} for any of our $YBa_2Cu_3O_7$ samples.[10-15] Other investigators have explored the relationship between the residual microwave loss and the submillimeter absorptivity deduced from reflectivity measurements. Our data are generally consistent with early work,[16] but not with a more recent paper which shows higher microwave losses relative to the infrared loss than we observe.[17] The losses measured for the thallium films also vary as frequency squared up to ~ 300 GHz above which strong phonon structure is observed. This is in strong contrast to the case for other high T_c superconductors such as $YBa_2Cu_3O_7$, where phonon structure observed in ceramic samples is absent

in epitaxial oriented films and crystals because of the electronic screening due to the high conductivity of the a-b planes.

2. Experimental Approach

In order to make a direct measurement of the absorptivity we have used the high-T_c film as the absorbing element in a composite bolometric far infrared detector.[18] The 250 - 500 μm thick substrates are suspended in a thermal vacuum by 100μm thick nylon threads. Typical substrates are 5 × 5 mm^2. The back surface of each substrate is coated with a gold film to reduce absorption of stray radiation and a small neutron transmutation doped (NTD) germanium thermistor [19] and NiCr heater [20] are glued to this surface. The ~100 ms thermal time constant τ = C/G of the bolometer is determined by the heat capacity C of the assembled bolometer and the thermal conductance G due to the electrical leads from the thermistor to the heat sink at 2K.

A schematic of the experimental apparatus is shown in Fig. 1. Infrared radiation (A) chopped at 10 Hz from a Fourier transform spectrometer operated in the step-and-integrate mode passes through a light pipe and a cold low pass filter to a roof mirror (B) which divides the beam symmetrically between the sample bolometer (I) and a reference bolometer with known absorptivity (II). The aperture (C) of a thin walled brass tube (not shown) which is pressed against the absorbing film defines the throughput $A\Omega \approx 0.03$ sr-cm^2 onto each film. The absorbing film is located on the front surface of the substrate (E) which is held firmly against the exit of the throughput limiter by tension in the nylon threads (F), which are suspended from a support ring (G). The absorbing films are electrically isolated from the throughput limiters and are surrounded by infrared absorber[21] (D) to reduce stray radiation. The support ring (G) also serves as a heat sink (L) for the electrical connections (H) to the thermistor (J) and heater resistor (K). Frequency dependent

asymmetries in the throughput are measured and corrected by interchanging sample and reference detectors.

The frequency dependence of the response to an ac current through the heater and to chopped infrared radiation are measured to confirm that all internal thermal relaxation times in the bolometer are much shorter than C/G. Under these conditions the responsivity R^f of the bolometer to absorbed infrared power at frequency f can be measured by passing an ac current at frequency $f/2$ through the known heater resistance.

The output spectrum from each detector channel can be represented by $F(v) = L(v) A(v) R^f$ where v is the wavenumber (cm^{-1}), $L(v)$ is the submillimeter spectrum incident on the absorbing film from the spectrometer, $A(v)$ is the absorptivity of the film, and R^f is the responsivity of the detector to absorbed power. If the detector responsivities and the absorptivity of the reference detector are known then the absorptivity of the sample can be determined from

$$A_s(v) = \frac{F_s(v)\ R_r^f}{F_r(v)\ R_s^f}\ A_r(v)\ ,$$

(1)

where the subscripts s and r refer to the sample and reference channels, respectively, and where $A_r(v)$ is the known absorptivity of the reference absorber.

The success of this experiment depends on the availability of a reference film with known absorptivity. In addition, the reference absorber should have a small heat capacity and an absorptivity comparable to that of the sample. For this reason we use a sputtered gold film. No special precautions are taken to insure the purity of the sputtered metal and so the conductivity of the film is low enough that the absorptivity can be calculated from the classical skin effect theory using the conductivity $\sigma(\omega) = \sigma_{dc} / (1 - i\omega\tau)$. Here $\sigma_{dc} = ne^2\tau/m$ is the dc conductivity of the

gold film measured at 4K and τ is the momentum relaxation time inferred from σ_{dc} assuming a free electron mass and a carrier density of one electron per atom.[22]

Because of surface imperfections the optical absorptivity calculated from the bulk dc properties will underestimate the actual film absorptivity.[23] In order to correct for this effect we have measured the absorptivity of an etched brass foil relative to the gold reference. By fitting the ratio of absorptivities of brass and gold to a Drude model for each of the materials we are able to determine an effective dc conductivity and carrier density for both the brass and the gold. The use of these effective parameters should then partially compensate for the effects of surface imperfections.

The absorptivity of the brass is calculated from the classical skin effect theory using the dc conductivity of the brass measured at 4K and the carrier density estimated from a room temperature Hall coefficient measurement [24] assuming a single carrier band. We calculate the ratio of the absorptivities of brass and gold from the respective dc material properties and also from a best fit to the measured infrared ratio. The measured infrared ratio and the absorptivity ratio determined from the dc properties of the brass and gold, as well as the best fit absorptivity ratio, are shown in Fig. 2 . A list of the dc and best fit parameters for the brass and the gold is given in Table I.

The agreement between the directly measured ratio and the ratio determined from the dc properties is quite good between 30 and 650 cm^{-1}; the agreement between the directly measured ratio and the best fit is excellent over the same frequency range. Because the optical data accounts more accurately for the actual surface properties of the gold film than the simple theory, we use the absorptivity of the gold film determined from the best fit of the optical data to characterize the gold film. The correction to the frequency dependent absorptivity of the gold film varies smoothly with frequency. At 30 (700) cm^{-1} the best fit absorptivity is 3%

higher (15% lower) than the absorptivity determined from the dc properties of the gold alone.

Deviations between the best fit and the absorptivity ratio in Fig. 2 help to establish the valid range of the optical data. The reproducibility of the data is poor above 650 cm^{-1}. This may reflect the sensitivity of the spectrometer to thermal drifts at these high frequencies. Deviations are seen below 30 cm^{-1} which appear to be due to the decreasing effectiveness of the light baffles surrounding the sample. The light baffles become transparent below ~30 cm^{-1}.[25] This effect leads to an overestimation of $A(\omega)$. Because the sample and reference absorptivities are not identical this error does not cancel out when the ratio of absorptivities is calculated.

As a test of the method we have measured the absorptivity of a 250 nm Nb film at 2K which is shown in Fig. 3. Note that we are able to observe a superconducting gap in the Nb at ~ 25 cm^{-1} where the absorptivity is less than 0.5%.

3. Results for Y-Ba-Cu-O films

The a-b plane oriented YBa$_2$Cu$_3$O$_7$ samples used in this study were and grown on MgO and LaAlO$_3$ substrates, as summarized in Table I. Samples A, B, C and E were produced by 90° off - axis sputtering,[26,27] and film D was produced by pulsed-excimer-laser deposition.[28,29]

The microwave surface resistance R$_s$ of samples A, B, C and E was measured at 11 - 13 GHz with a parallel plate resonator technique.[5] The surface resistance of sample D was measured in a superconducting niobium cavity operated in the TE$_{011}$ mode at 5.95 GHz.[6] We have analyzed the effect of the finite film thickness on the measurement by extending the treatment of Klein et al. [30] to 10 GHz and 4 K using λ = 140 nm. We find that measured surface impedances at 10 GHz and 4K are only weakly dependent on film thickness for films thinner than ~400 nm so that no

corrections to the measured surface resistances is required. We have done similar calculations at higher frequencies up to 1 THz, corresponding to the lowest frequencies of the submillimeter absorptivity measurement, and also find that no correction to the measured absorptivity is required for the range of measured absorptivities and film thicknesses studied.

The $YBa_2Cu_3O_7$ samples used in this study are notable for their lack of impurity phase and high degree of epitaxial alignment perpendicular to their surface, with the $YBa_2Cu_3O_7$ c-axis perpendicular to the substrate surface. Compositional analysis with Rutherford backscattering spectrometry indicated that the films used in this study were in the 1:2:3 phase.[26,31,32] Crystalline quality was studied by measuring x-ray rocking curve widths for films nominally identical to those used in this study [27,29,31,33,34] and suggest within the limitations of the experiment that these films have nearly perfect single crystalline structure. However, transmission and scanning electron microscopy studies indicate that these films are heavily faulted.[29]

The microstructure of the laser deposited films on $LaAlO_3$ exhibit undulations both along the (001) planes (c-layers) and the (110) planes, with a typical structural correlation range of about 10 nm.[29] These films are nevertheless free from macroscopic grain boundaries [10,29,31] and are very homogeneous, with surface roughness less than 15 nm, and are free from any secondary phase.[29,35] Typical c-axis oriented films deposited by off-axis sputtering exhibit a high density of intersecting (110) twins, with typical spacings ranging from 10 - 70 nm and with twin lengths from 20 - 200 nm.[32] Typical surface roughness for c-axis films deposited onto MgO is less than 5 nm.[32] Films deposited on $LaAlO_3$ can be rougher.[34] In addition, the off-axis sputtered films contain a small volume fraction of a-axis oriented grains,[32,34] typically less than 1%.

In-plane film texture was examined by studying x-ray ϕ scans.[36] Both LaAlO$_3$ and the 1:2:3 phase of YBa$_2$Cu$_3$O$_7$ have a perovskite structure and the lattice match between these materials is good. However, a 7-9% lattice mismatch for MgO and YBa$_2$Cu$_3$O$_7$ in the (001) crystallographic direction may, under non-optimal growth conditions, lead to the formation of grains in which the in-plane unit cell axis of the film is aligned with the (110) axis of the substrate, corresponding to a rotation of 45°. The size of these 45° rotated domains ranges from 0.5 to 10.0 μm.[32] Off-axis sputtered films on MgO typically contain less than 1% volume fraction of such misoriented grains and misorientations of other distinct angles.[32]

The results of our measurements are shown in Fig. 4 along with two theoretical fits described below. The curves are displaced by factors of ten to avoid overlap. The filled circles give the microwave loss measurements at 4K. The size of the circles is large enough to include estimated errors. The solid lines give the submillimeter absorptivity measurements at 2K. Additive errors are thought to be small down to the lowest frequencies presented. Multiplicative errors could be as large as 15 percent. These results give a picture of the residual loss in epitaxial a-b plane YBa$_2$Cu$_3$O$_7$ films over nearly four orders of magnitude in frequency. In each case, the 10 GHz point can be connected to the submillimeter data by a line which varies as frequency squared. This agrees with observations by others[8] in the range from 10 to ~100 GHz (0.3-30 cm^{-1}). The frequency dependence of the loss saturates smoothly above ~600 GHz (20 cm^{-1}) in a way that is different for different films. There is no sign of any gap-like onset of absorption near 2.1 kT$_c$ as reported in some early work [13] or near the BCS value of 3.5 kT$_c$ = 6.6 THz (220 cm^{-1}). There is a sharp onset of absorption at 13.5 THz (450 cm^{-1}) or 7.2 kTc in our high quality films that has been seen by others in reflectivity experiments.[11,14] Although it seems not to be a BCS-like energy gap, there is clearly a very sudden onset of some additional absorption mechanism. Other investigators have explored the relationship

between the residual microwave loss and the submillimeter absorptivity deduced from reflectivity measurements. Our data are generally consistent with early work,[16] but not with a more recent paper which shows higher microwave losses relative to the infrared loss than we observe.[17]

Because of the low critical field H_{c1} for the ceramic superconductors it is certain that there is trapped flux in thin films at low temperatures due to the laboratory magnetic field. Flux motion driven by the incident radiation is a potential source of the loss in these films. In order to explore this effect, fields of approximately 10 Gauss were applied normal to the films with both the smallest and largest microwave R_s and fields of up to 3.5 T were applied normal to film B. No significant differences in the measured absorptivities were observed.

We have used two models of residual loss to fit our data below the absorption edge at 13.5 THz. The first is the model proposed by Hylton et al.[37,38] that treats polycrystalline high-T_c films as networks of weakly coupled grains, where the material of the grains is an ideal BCS superconductor. The grain boundaries form resistively shunted Josephson junctions with critical current density j_c, shunt resistance ρ_J/a and equivalent Josephson penetration depth λ_j. The grains have characteristic size a and superconducting penetration depth λ_g. The magnetic field profile averaged over individual grains is given by $\lambda_{eff} = (\lambda_g^2 + \lambda_j^2)^{1/2}$. This model predicts a frequency squared dependence of the losses at low frequencies and frequency independent losses at high frequencies. The data below 13.5 THz do not contain enough information to uniquely determine the three independent parameters in this model. Consequently, we use the penetration depth obtained from muon spin rotation (μsr) experiments[39] to constrain the fit. This procedure is complicated by the interpretation of the μsr data for inhomogeneous materials. In principle, μsr measures the volume-weighted distribution of magnetic fields throughout the sample. There is a tendency to focus

on the rather narrow distribution of fields in the grains which comprise most of the sample volume rather than the broader distribution of fields in the grain boundaries which comprise a much smaller volume. To the extent that this is the case, the μsr experiment measures λ_g, and not λ_{eff}. The fitting is done by characterizing the submillimeter data below 13.5 THz by 20 points equally spaced in log frequency and the microwave data by one point. The two remaining free parameters are then determined by a chi squared minimization technique.

The fits to the weakly coupled grain model, constrained by the μsr measurement[39] with λ_g = 140 nm, are shown in Fig. 4 as the long dashed lines. The weakly coupled grain model is able to fit the data for all five films measured. The results of the fit are given in Table III. Values for the product of the critical current times the resistance $I_cR = \hbar c^2 \rho_J / 8\pi\lambda_J^2 e$ ranges from 3 to 11 mV for the grain boundaries in our films. This can be compared with a range of 0.2 to 8 mV measured for grain boundary junctions at 4.2K.[40] If we assume that the critical current density j_c of the grain boundaries is essentially the critical current density 3×10^7 A cm^{-2} of the films,[32] then the characteristic grain size $a = I_cR/\rho_J j_c$ ranges from 4 to 40 nm in our films. This range is roughly consistent with the spatial correlation range in the laser ablated films of ~ 10 nm,[29] and with twin domain sizes in off-axis sputtered films of ~ 20-200 nm.[32] These values of a are considerably smaller than the typical 0.5 to 10 μm size range of the 45° grains in off-axis sputtered films on MgO.[32] Although such high angle grain boundaries are known to behave as resistively shunted junctions[40] which could therefore justify the use of the weakly coupled grain model, the volume fraction of such grains in our films is typically less than one percent.[32,33] Nevertheless, the parameter values deduced from fitting the weakly coupled grain model are reasonable considering the simplicity of the model. Furthermore, the frequency dependent conductivity $\sigma(\omega)$ obtained from the weakly coupled grain model is in good agreement with $\sigma(\omega)$

obtained from the Kramers-Kronig transform of our loss data for all films measured.[1,41].

Because the interpretation of the μsr experiments in terms of λ_g is somewhat ambiguous, we have also studied the fit obtained when we constrain λ_{eff} = 140 nm. The best fits shown in Fig. 4 as short dashed lines are acceptable for some, but not all of our films. In the case of film E which has high residual loss, the fit does not even intersect the data. The fit can be forced to intersect the data, but the resulting slope at high frequencies is then so small that the value of chi squared is degraded.

We have also used a type of homogeneous two-fluid model to fit the data which assumes that a fraction of the conduction electrons does not condense into the superconducting state, even at our low temperatures. This model yields a fitting function with the same mathematical form as the weakly coupled grain model.[1,2] When we constrain the superconducting penetration depth in the two fluid model, λ_{tf} = 140 nm, we get exactly the same unsatisfactory fit (shown by the short dashed lines in Fig. 4) as when we set λ_{eff} = 140 nm in the weakly coupled grain model. In addition, the agreement between the conductivity $\sigma(\omega)$ obtained from the two fluid model is in poor agreement with $\sigma(\omega)$ obtained from the Kramers-Kronig transform of our loss data for all films measured.[1,41]

4. Results for Tl-Ba-Ca-Cu-O films

The a-b plane oriented Tl-Ba-Ca-Cu-O samples used in this study were and grown on LaAlO$_3$ substrates, as summarized in Table II. Samples L1 and L2 were produced by 90° off - axis sputtering onto LaAlO$_3$ substrates from sintered targets prepared from oxide powder mixtures with an initial cation ratio of 2Tl:2Ca:2Ba:3Cu. These amorphous precursor films were subsequently wrapped with 2:2:2:3 pellets and post-annealed at ~ 850 °C in order to minimize Tl$_2$O$_3$ loss. This technique has been described previously.[42] Film S1 was prepared by a laser

ablation technique followed by a post-deposition thermal process at 830 - 900°C under controlled Tl and oxygen pressure to minimize loss of Tl_2O_3.[43]

The microwave surface resistance for samples L1 and L2 were measured at 11 - 13 GHz with a parallel plate resonator technique[5] and the microwave surface resistance for samples L1, L2 and S1 were measured at 30 and 90 GHz with a confocal resonator technique.[7] We do not expect corrections to the measured surface resistance due to film transparency to be significant.[30]

Film microstructure for one of the samples (L2) was investigated using a four circle x-ray diffractometer. Within experimental uncertainty, the x-ray $\theta/2\theta$ scan indicates that for this film as much as 70% but as little as 30% of the oriented material is in the 2:2:2:3:10 phase, with the remainder of the oriented material in the 2:1:2:2 phase, where the c-axis is perpendicular to the substrate surface. X-ray $\theta/2\theta$ scans on similar films indicates that as much as 80% of the oriented material may be in the 2:2:2:3 phase. However, the relatively high background suggests the presence of some volume fraction of amorphous or randomly oriented polycrystalline grains. The x-ray ϕ scan on the same film indicates that the c-axis oriented 2:2:2:3:10 and 2:1:2:2:8 phase material in these films are in excellent registry with the $LaAlO_3$ substrate. X-ray $\theta/2\theta$ scans on samples nominally identical to film S1 indicate that this is a single 2:1:2:2:8 phase film and is c-axis oriented. Sharp x-ray rocking curves indicate that film S1 is epitaxially oriented on the $LaAlO_3$ substrate.[43] Scanning electron microscopy on films similar to L1,L2 and S1 show a lateral defect structure in the a-b plane with spacing on the order of ~10 μm. Tunneling electron microscopy on films similar to S1 indicate that these defects have typical depth of ~ 100 nm.

The submillimeter absorptivity spectra for epitaxial films L1 and L2 are plotted in Fig. 5. The submillimeter spectra contain many phonon modes between 2 and 21 THz. Such phonon structure has previously been observed

experimentally in the sintered ceramic sample of Zetterer et $al.$, which is also plotted in Fig. 3.[44] Our films exhibit remarkably similar structure to that observed in the ceramic sample between 2 and 21 THz. Therefore the agreement with lattice vibration calculations found for the phonon structure from the sintered ceramic[44] should also be valid for the structure we measured on the films. However, the overall absorptivity of the epitaxial films is lower than for the ceramic samples.

We expect the high conductivity of the a-b plane to screen out phonon excitations with vibrational motion in the a-b plane. We therefore believe that the phonon modes observed in epitaxial films L1 and L2 correspond to infrared active excitations perpendicular to the a-b plane. The observed phonon structure is in agreement with a lattice dynamical study which show the existence of 8 phonon modes for 2:2:2:3 phase material with $E \parallel c$.[45] Since the incident fields probing the sample in our measurement are predominantly parallel to the surface of the film, the plausible identification of the observed structure to $E \parallel c$ phonon modes suggest the presence either of a substantial fraction of the film containing grains whose c-axis is not perpendicular to the film surface or of considerable surface roughness which would cause current to be driven along the c direction. For films L1 and L2, the former possibility is consistent with the observation of a large background in the x-ray $\theta/2\theta$ scan measured for film L2.

The losses for films L1 and L2 are again plotted with the losses for film S1 in Fig. 6 (solid lines) along with the microwave loss data (filled circles) measured for the same films near 10 K. The curves in Fig. 6 are displaced by factors of 10 to avoid overlap. The size of the circles are large enough to include measurement uncertainties and possible corrections for film transparency. The dotted lines in Fig.

6 are frequency squared best fits to the microwave data. Losses at low frequencies increase as frequency squared between 10 and 90 GHz and are in good agreement with submillimeter data for both films. For all thallium films studied, the microwave data can be connected to the submillimeter data at ~ 1 THz by a line which goes as $\omega^{2-\delta}$ where $\delta <<$ 1. This suggests that the losses at the lowest frequency of the submillimeter measurement have not saturated to the ω^2 limit. Submillimeter losses for film S1 also show strong phonon structure between 1 and 21 THz, which is consistent with lattice dynamical calculations.[45] We tentatively attribute the phonon structure in film S1 to c-axis modes for the same reasons given for films L1 and L2. In contrast to films L1 and L2, the occurence of this phonon structure is not consistent with the presence of randomly oriented grains, since x-ray rocking curve studies suggest that film S1 is highly epitaxial. However, there is considerable surface roughness in these films, approximately 100 nm. In this case current induced in the a-b plane by the incident fields could cause current to be driven along the c direction which explain the presence of these c-axis phonon modes.

5. Conclusions

We have characterized the residual loss in epitaxial a-b plane films of $YBa_2Cu_3O_7$, $Tl_2CaBa_2Cu_2O_8$ and mixed phase $Tl_2Ca_2Ba_2Cu_3O_{10}$ and $Tl_2CaBa_2Cu_2O_8$ films from 10 GHz to 21 THz. We do not observe any gap-like features below 15 THz for any of the films studied. For all films studied the losses below ~ 1 THz scale approximately as frequency squared.

We have shown that the frequency dependence of the loss below 13.5 THz for the $YBa_2Cu_3O_7$ films can be well represented by a weakly coupled grain model if the penetration depth in the grains λ_g is set equal to 140 nm. Because this model is strictly valid at frequencies below the superconducting gap, our model fitting

implicitly assumes that the superconducting energy gap 2Δ, if one exists, either occurs at or above 450 cm^{-1}, or makes no contribution to the absorptivity. In addition, we find remarkable agreement between the results of a Kramers-Kronig analysis and the best fits from the weakly coupled grain model below 450 cm^{-1} for all films. These results suggest that weak link behavior may play a significant role in the microwave and submillimeter losses. Values of junction $I_c R$ products and a characteristic length determined from the model best fits are consistent with these independently measured quantities.

We are unable to fit the losses in the Tl-Ba-Ca-Cu-O films to the weakly coupled grain model. We observe strong phonon structure in the Tl-Ba-Ca-Cu-O films between 1 and 21 THz. This is in strong contrast to the case for other high T_c superconductors such as $YBa_2Cu_3O_7$, where phonon structure observed in ceramic samples is absent in epitaxial oriented films and crystals because of the electronic screening due to the high conductivity of the a-b planes.

References

1. D. Miller, P.L. Richards, S. Etemad, A. Inam, T. Venkatesan, B. Dutta, X.D. Wu, C.B. Eom, T.H. Geballe, N. Newman and B.F. Cole, (submitted to Phys. Rev. B)

2. D. Miller, P.L. Richards, S. Etemad, A. Inam, T. Venkatesan, B. Dutta, X.D. Wu, C.B. Eom, T.H. Geballe, N. Newman and B.F. Cole, Appl. Phys. Lett. **59**, 2326 (1991)

3. T. Pham, H.D. Drew, S.H. Moseley and J.Z. Liu, Phys. Rev. B **41**, 11681 (1990)

4. T. Pham, M.W. Lee, H.D. Drew, U. Welp and Y. Fang, Phys. Rev. B **44**, 5377 (1991)

5. R.C. Taber, Review of Scientific Instruments **61**, 2200 (1990)

6. H. Padamsee, J. Kirchgessner, D. Moffat, J. Potts, D.L. Rubin, Q.S. Shu, A. Inam, X.D. Wu, L. Nazar, M.S. Hegde and T. Venkatesan, (unpublished)

7. J.S. Martens, V.M. Hietala, D.S. Ginley, T.E. Zipperian and G.K.G. Hohenwarter, Appl. Phys. Lett. **58**, 2326 (1991)

8. H. Piel and G. Muller, IEEE Trans. Magn. **27**, 854 (1991)

9. C.M. Foster, K.F. Voss, T.W. Hagler, D. Mihailovic, A.J. Heeger, M.M. Eddy, W.L. Olson and E.J. Smith, Sol. State Comm. **76**, 651 (1990)

10. K. Kamaras, L.L. Herr, C.D. Porter, N. Tache, D.B. Tanner, S. Etemad, T. Venkatesan, E. Chase, A. Inam, X.D. Wu, M.S. Hegde and B. Dutta, Phys. Rev. Lett. **64**, 84 (1990)

11. J. Orenstein, G.A. Thomas, A.J. Millis, S.L. Cooper, D.H. Rapkine, T. Timusk, L.F. Schneemeyer and J.V. Waszczak, Phys. Rev. B **42**, 6342 (1990)

12. Z. Schlesinger, R.T. Collins, F. Holtzberg, C. Field, G. Koren and A. Gupta, Phys. Rev. B **41**, 11237 (1990)

13. J. Schutzmann, W. Ose, J. Keller, K.F. Renk, B. Roas, L. Schultz and G. Saemann-Ischenko, Europhys. Lett. **8**, 679 (1989)

14. B. Batlogg, in <u>High Temperature Superconductivity Proceedings, Los Alamos Symposium 1989</u>, edited by K. S. Bedell, D. Coffey, D. E. Meltzer, D. Pines and J. R. Schrieffer (Addison-Wesley, California, 1990), p. 37

15. T. Timusk and D.B. Tanner, in Physical Properties of High Temperature Superconductors I , edited by D. M. Ginsberg (World Scientific, New Jersey, 1989), p. 339

16. K.F. Renk, J. Schutzmann, A. Pruckl, B. Roas, L. Schultz and G. Saemann-Ischenko, Physica B 165&166, 1253 (1990)

17. K.F. Renk, B. Gorshunov, J. Schutzmann, A. Pruckl, B. Brunner, J. Betz, S. Orbach, N. Klein, G. Muller and H. Piel, Europhys. Lett. 15, 661 (1991)

18. N.S. Nishioka, P.L. Richards and D.P. Woody, Appl. Opt. 17, 1562 (1978)

19. E.E. Haller, Infrared Phys. 25, 257 (1985)

20. NiCr resistors are manufactered by Mini-Systems Inc., North Attleboro, Mass. 02761

21. The infrared absorber is made from precast Eccosorb CR110, Emerson and Cuming, Gardena, CA, USA

22. C. Kittel, Introduction to Solid State Physics , (Wiley, New York, 1986)

23. R.G. Chambers and A.B. Pippard, Institute of Metals Monograph 13, 281 (1953)

24. W. Koster and H.P. Rave, Z. Metallkde. 55, 750 (1964)

25. M. Halpern, H.P. Gush, E. Wichnow and V. deCosmo, Appl. Opt. 25, 565 (1986)

26. N. Newman, K. Char, S.M. Garrison, R.W. Barton, R.C. Taber, C.B. Eom, T.H. Geballe and B. Wilkens, Appl. Phys. Lett. 57, 520 (1990)

27. C.B. Eom, J.Z. Sun, K. Yamamoto, A.F. Marshall, K.E. Luther and T.H. Geballe, Appl. Phys. Lett. 55, 595 (1989)

28. A. Inam, M.S. Hegde, X.D. Wu, T. Venkatesan, P. England, P.F. Miceli, E.W. Chase, C.C. Chang, J.M. Tarascon and J.B. Wachtman, Appl. Phys. Lett. 53, 908 (1988)

29. D.M. Hwang, T. Venkatesan, C.C. Chang, L. Nazar, X.D. Wu, A. Inam and M.S. Hegde, Appl. Phys. Lett. 54, 1702 (1989)

30. N. Klein, H. Chaloupka, G. Muller, S. Orbach, H. Piel, B. Roas, L. Schulz, U. Klein and M. Peiniger, Journal of Applied Physics 67, 6940 (1990)

31. A. Inam, X.D. Wu, L. Nazar, M.S. Hegde, C.T. Rogers, T. Venkatesan, R.W. Simon, K. Daly, H. Padamsee, J. Kirchgessner, D. Moffat, D. Rubin, Q.S. Shu, D. Kalokitis, A. Fathy, V. Pendrick, R. Brown, B. Brycki, E. Belohoubek, L.

Drabeck, G. Gruner, R. Hammond, F. Gamble, B.M. Lairson and J.C. Bravman, Appl. Phys. Lett. **56**, 1178 (1990)

32. C.B. Eom, J.Z. Sun, B.M. Lairson, S.K. Streiffer, A.F. Marshall, K. Yamamoto, S.M. Anlage, J.C. Bravman, T.H. Geballe, S.S. Laderman, R.C. Taber and R.D. Jacowitz, Physica C **171**, 354 (1990)

33. S.S. Laderman, R.C. Taber, R.D. Jacowitz, J.L. Moll, C.B. Eom, T.L. Hylton, A.F. Marshall, T.H. Geballe and M.R. Beasley, Phys. Rev. B **43**, 2922 (1991)

34. N. Newman, B.F. Cole, S.M. Garrison, K. Char and R.C. Taber, IEEE Trans. Magn. **27**, 1276 (1991)

35. T.S. Ravi, D.M. Hwang, R. Ramesh, S.W. Chan. L. Nazar, C.Y. Chen, A. Inam and T. Venkatesan, Phys. Rev. B **42**, 10141 (1990)

36. J. Sizemore, R. Barton, A. Marshall, J.C. Bravman, M. Naito and K. Char, IEEE Trans. Magn. **25**, 2245 (1989)

37. T.L. Hylton, A. Kapitulnik, M.R. Beasley, J.P. Carini, L. Drabeck and G. Gruner, Appl. Phys. Lett. **53**, 1343 (1988)

38. T.L. Hylton and M.R. Beasley, Phys. Rev. B **39**, 9042 (1989)

39. D.R. Harshman, L.F. Schneemeyer, J.V. Waszczak, G. Aeppli, R.J. Cava, B. Batlogg, L.W. Rupp, E.J. Ansaldo and D.L. Williams, Phys. Rev. B **39**, 851 (1989)

40. R. Gross, P. Chaudhari, M. Kawasaki and A. Gupta, IEEE Trans. Magn. **27**, 3227 (1991)

41. D. Miller and P.L. Richards, (submitted to Phys. Rev. B)

42. W.Y. Lee, S.M. Garrison, M. Kawasaki, E.L. Venturini, B.T. Ahn, R. Boyers, J. Salem, R. Savoy and J. Vazquez, Appl. Phys. Lett. **60**, 772 (1992)

43. R.B. Hammond, G.B. Negrete, L.C. Bourne, D.D. Strother, A.H. Cardona and M.M. Eddy, Appl. Phys. Lett. **57**, 825 (1990)

44. T. Zetterer, M. Franz, J. Schutzmann, W. Ose, H.H. Otto and K.F. Renk, Phys. Rev. B **41**, 9499 (1990)

45. A.D. Kulkarni, F.W. DeWette, J. Prade, U. Schroder and W. Kress, Phys. Rev. B **41**, 6409 (1990)

Table I: $YBa_2Cu_3O_7$ samples measured in this work. Values of the microwave surface resistance R_s measured near 4K and 10 GHz are scaled to 10 GHz using an ω^2 law, where ω is the microwave frequency. T_c's are measured from midpoint of transition; widths are measured from 10 - 90 % of transition. Sample E was intentionally grown to have large microwave loss.

Sample	Institution	thickness (nm)	Substrate	Tc/δT (K)	Deposition Technique	R_s (μΩ)
A	Stanford	500	MgO	85 / 1.0	Off-Axis Sputter	12
B	Stanford	400	MgO	85 / 1.0	Off-Axis Sputter	16
C	Conductus	410	$LaAlO_3$	87 / 1.0	Off-Axis Sputter	30
D	Bellcore	500	$LaAlO_3$	92 / 0.5	Laser Ablation	48
E	Conductus	1250	$LaAlO_3$	87 / 2.0	Off-Axis Sputter	180

Table III: Tl-Ca-Ba-Cu-O samples measured in this work. Values of microwave surface resistance R_s measured at 4K near 10 GHz are scaled to 10 GHz using an ω^2 law, where ω is the microwave frequency. T_c's are measured from midpoint of transition; widths are measured from 10 - 90 % of transition. Films were grown on $LaAlO_3$ substrates.

Sample	Institution	thickness (nm)	Nominal Composition	$T_c/\delta T$ (K)	Deposition Technique	R_s ($\mu\Omega$)
L1	IBM	500	2:2:2:3:10	123 / 1.5	Off-Axis Sputter	84
L2	IBM	500	2:2:2:3:10	123 / 1.5	Off-Axis Sputter	84
S1	STI	700	2:1:2:2:8	~100 / 1.0	Laser Ablation	130

Table III: Parameters from weakly coupled grain model best fit to the absorptivity data for $YBa_2Cu_3O_7$ samples A through E with λ_g= 140 nm.

Sample	λ_{eff} (nm)	I_cR (mV)	a [a] (nm)
A	204 ± 12	11.0 ± 2.5	40 ± 10
B	224 ± 23	4.9 ± 1.2	29 ± 12
C	299 ± 49	8.0 ± 2.1	12 ± 5
D	212 ± 15	4.2 ± 0.9	34 ± 10
E	521 ± 96	3.1 ± 0.6	4 ± 1

[a] Values of the effective grain length, a, are calculated assuming $j_c = 3 \times 10^7$ A cm^{-2}

Figure Captions

FIG. 1.   Cross section of the apparatus, which was operated in a thermal vacuum at ~2 K. Incident radiation A is split by roof mirror B and sent to detector channels I and II. In each channel a throughput limiter C defines the incident radiation. Stray radiation is absorbed by baffles D. The film being measured is located on the front inner surface of a substrate E which is suspended by nylon threads F from the support ring G. Thermistors J and resistance heaters K are indicated schematically. Electrical connections H to thermistors and resistors provided the thermal conductance between the substrate and the heat sinks L.

FIG. 2.   Ratio of the measured absorptivity of brass and gold, as described in text. The solid line is the experimental data. The dashed line is the best fit of the Drude model to the data. The dash - dot line is the fit of the Drude model using the measured dc properties of the brass and gold.

FIG. 3.   Measured absorptivity of Nb thin film at 2K. The residual resistivity ratio for this film is ~ 6 - 7, and the microwave loss is nominally 20 $\mu\Omega$ at 4K and 10 GHz.

FIG. 4.   Measured submillimeter absorptivities of samples A through E at 2K (solid lines) multiplied by the indicated factors to separate the curves. Values of the microwave surface resistance are shown as filled circles are measured for each sample at 4K at the frequency indicated. Also shown are best fits to the weakly coupled grain model (long dashed lines) with λ_g = 140 nm and best fits to
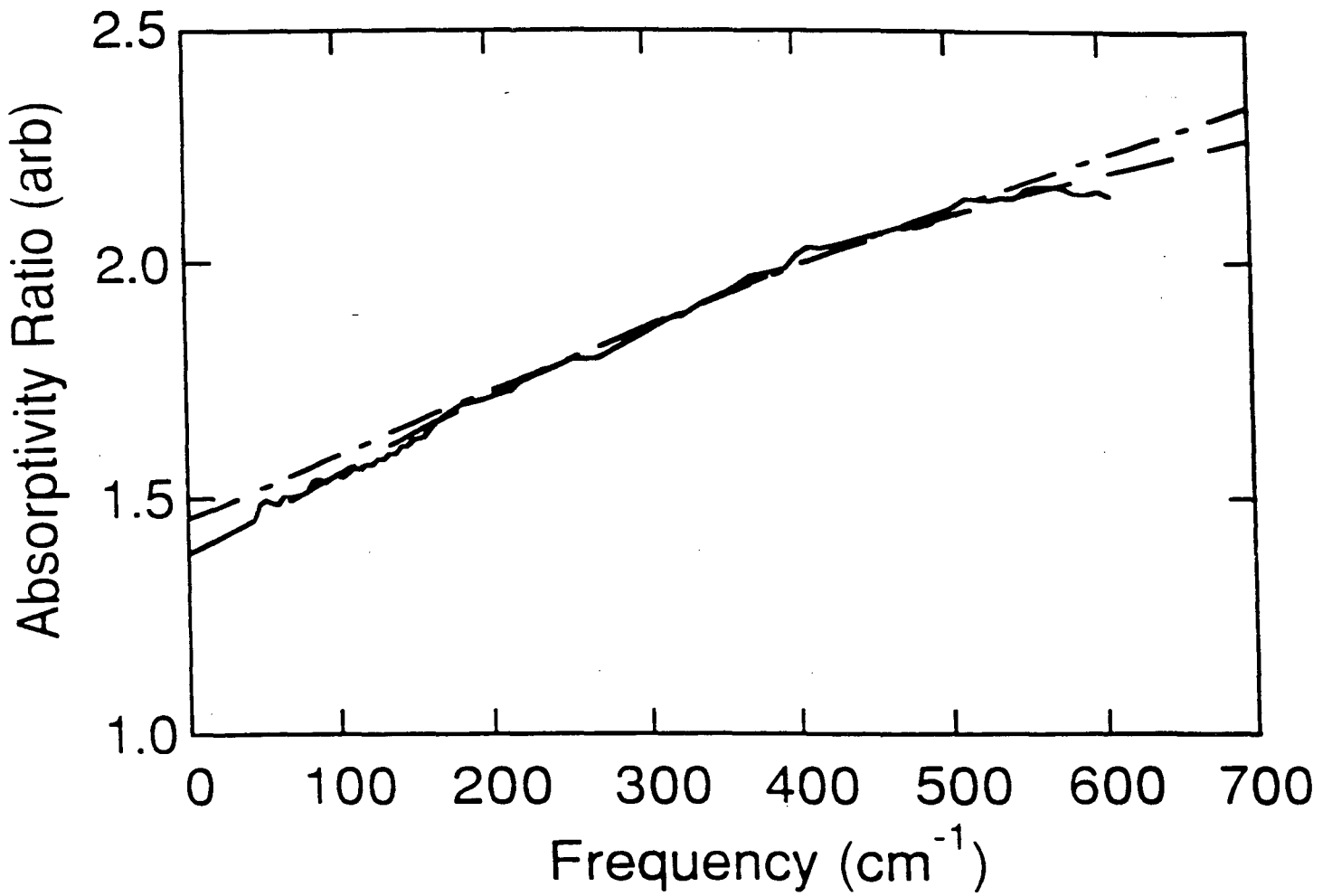
the two-fluid model (short dashed lines) with λ_{tf} = 140 nm. Sample E was intentionally prepared to give large microwave loss.
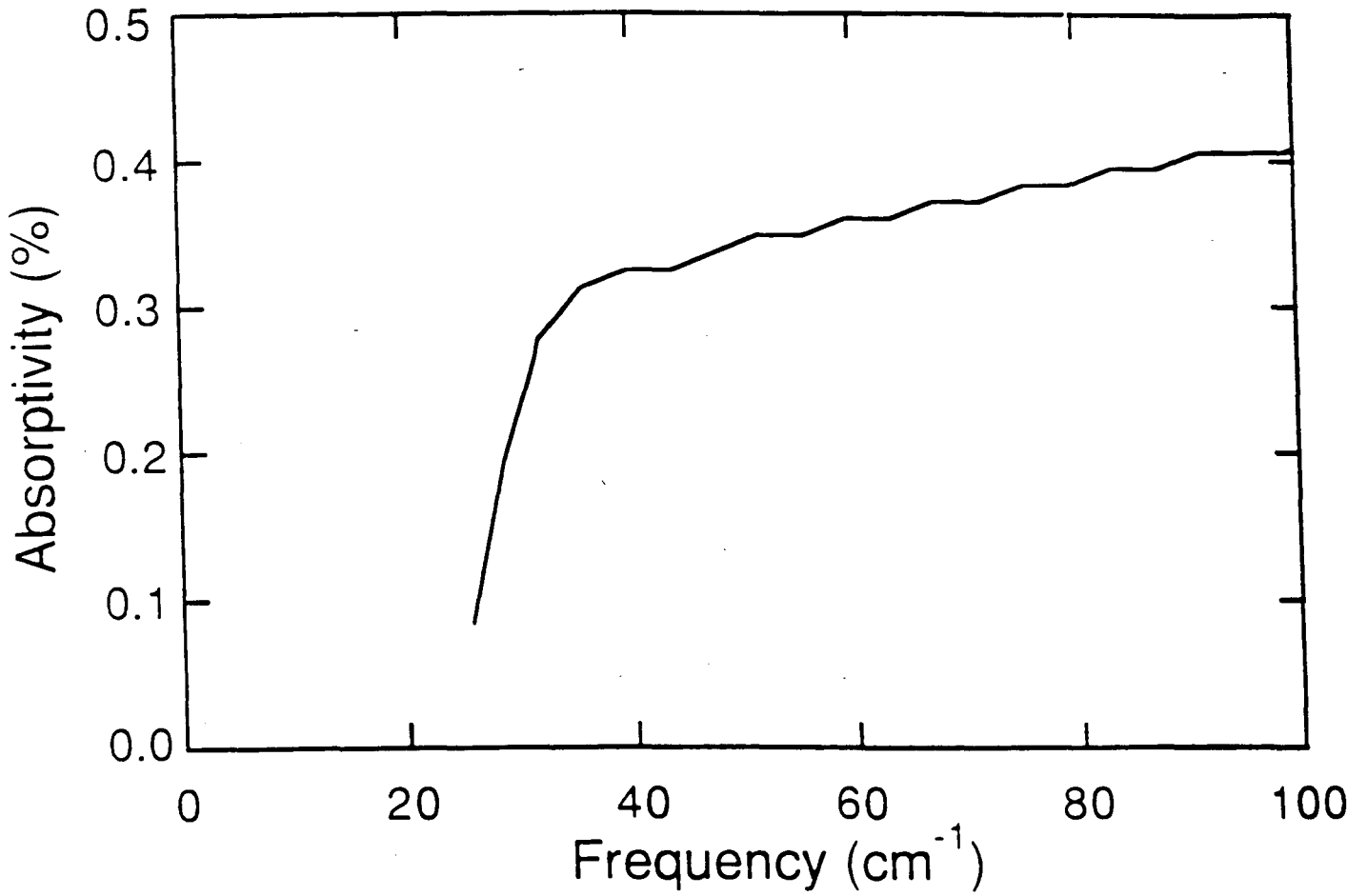
Fig. 5.   Submillimeter absorptivity spectra for the epitaxial $Tl_2Ca_2Ba_2Cu_3O_{10}$ samples L1 and L2 plotted logarithmically. Note that these films contain some volume fraction of the 2:1:2:2:8 phase. Also shown is the reflectivity measured by Zetterer *et al.* for a $Tl_2Ca_2Ba_2Cu_3O_{10}$ sintered ceramic sample plotted as an absorptivity. All three data sets show 8 phonon modes, in agreement with calculations for 2:2:2:3:10 phase material with E l l c.
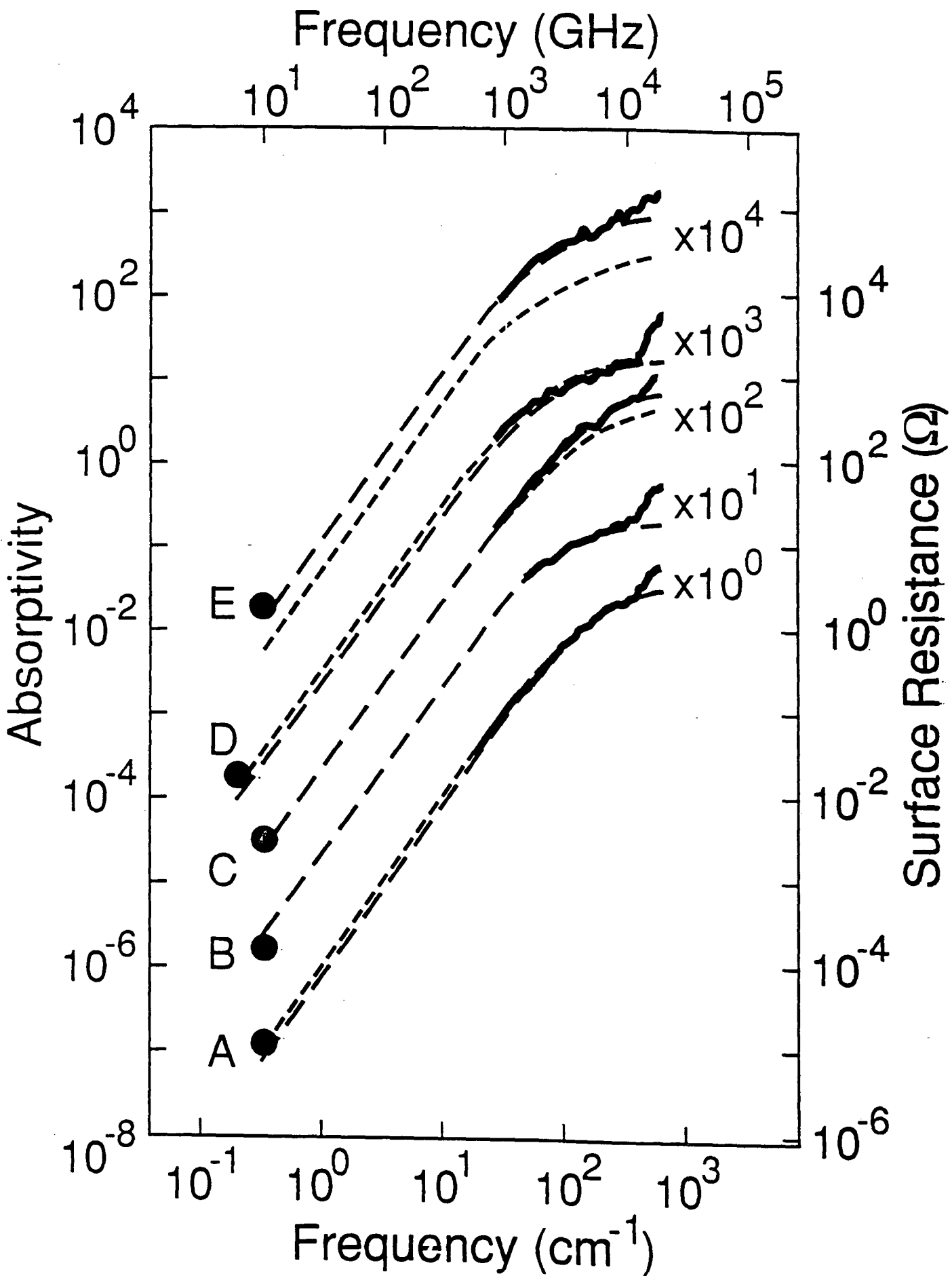
FIG. 6.   Measured submillimeter absorptivities of samples L1, L2 and S1 at 2K (solid lines) multiplied by the indicated factors to separate the curves. Values of the microwave surface resistance measured for each sample near 4K are shown as filled circles. The dotted lines are best fits to the microwave surface resistance data using an ω^2 dependence, where ω is the microwave frequency.
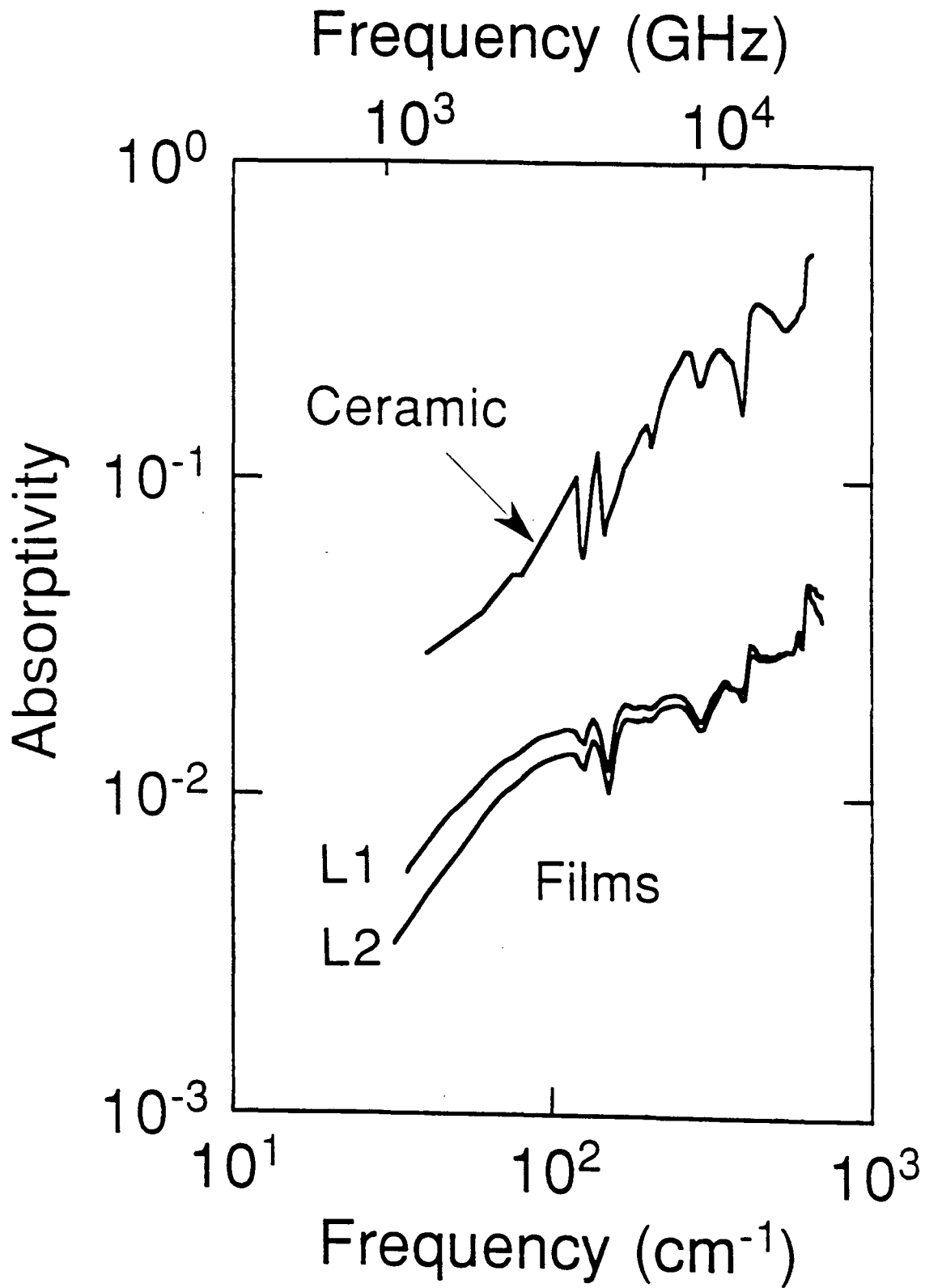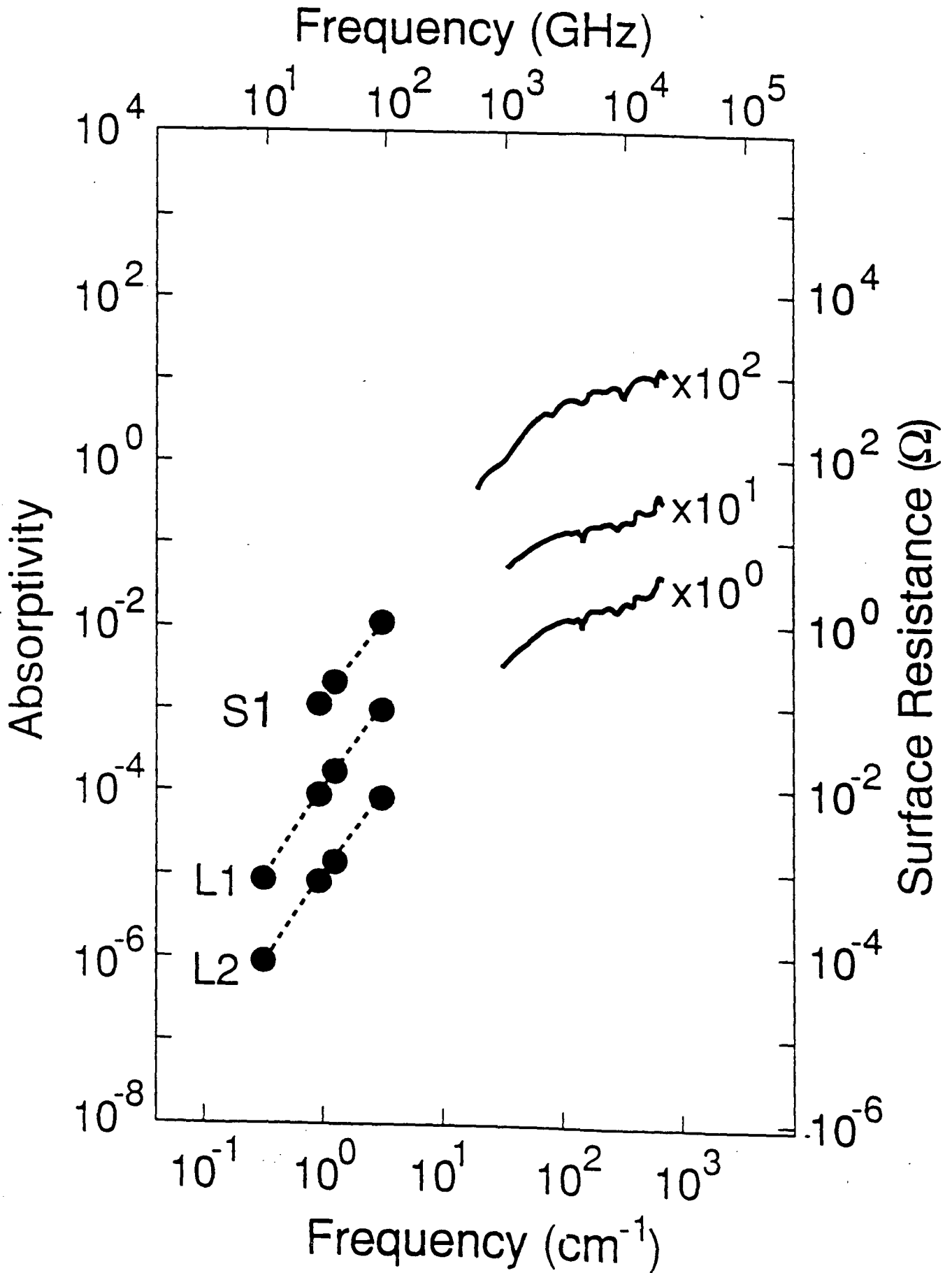
XBL 915-1040

XBL 919-2014

XBL 919-2015